Control of Free-Radical Emulsion Polymerization of Methyl Methacrylate by Oxygen Injection. I. Modeling Study

BRIAN M. LOUIE, WEN YEN CHIU, and DAVID S. SOONG,
Department of Chemical Engineering, University of California, Berkeley, California 94720

Synopsis

Oxygen injection has been proposed as an effective control measure for limiting the rate of heat release and altering the rate of polymerization in emulsion processes. A detailed mathematical model is developed to describe the system behavior with and without oxygen injection. Because of the rapid penetration of dissolved oxygen into the polymer particles, growing radical chains are terminated prematurely, lowering product molecular weights. Moderate oxygen flows and moderate set point temperatures are found to give the optimal response without significant lowering of the final molecular weight.

INTRODUCTION

Oxygen has long been known to inhibit free-radical polymerizations. In the early 1940s, operators at I.G. Farben were surprised by the top of an emulsion reactor blowing off when they used a stream of nitrogen for agitation in a normally aerated reactor. At about the same time, researchers at DuPont noted marked induction times when MMA was polymerized under an atmosphere of oxygen. They found that at high temperatures (around 60°C) there was little polymerization even in the presence of good initiators as long as the monomer was oxygenated by bubbling through air or by continuous agitation with splashing in an open reactor.[1]

This strong inhibition action can be used to temporarily curb the polymerization. Since polymerization is highly exothermic, programmed oxygen injection is proposed as a viable method for temperature control. The injected oxygen is assumed to permeate throughout the system rapidly, effectively terminating the majority of the growing radicals in the polymer particles, while simultaneously inactivating some of the aqueous phase radicals. This radical scavenging effect reduces the rate of conversion and heat release. Tight reactor control may thus be achieved.

The primary application of oxygen control is to rapidly alter existing reaction conditions inside a continuous emulsion polymerization train. These processes mainly suffer from thermal effects (ignition and runaway), oscillations in particle generation, and changes in steady state. These problems can be traced to poor control of the rate of polymerization. Rather than study such a train of reactors, a nonisothermal batch system will be examined experimentally. A batch reactor is chosen for this preliminary

Journal of Applied Polymer Science, Vol. 30, 3189–3223 (1985)
 CCC 0021-8995/85/083189-35$04.00

feasibility study because (1) it is easier to operate than a continuous process, (2) the whole range of conversion can be studied, (3) the fundamental phenomena governing the oxygen-controlled polymerization remain the same as the reference case with no oxygen present, and (4) flow configuration in a large CSTR train approaches that of a plug flow (or batch) reactor so that oxygen flows can be directly applied to a steady state train with limited cooling capacity.

Another application of oxygen control is to moderate the gel effect during the later stages of a batch or semibatch polymerization. Monomer loading per batch is usually limited by the rate of heat removal, and loadings are low because of the large amounts of heat released during the autoacceleration. Higher loadings are possible if heat transfer can be improved or heat generation controlled. Several possibilities exist. For example, cooling water flow in an external cooling jacket may be increased, or colder cooling water circulated to improve heat transfer. A chain transfer agent may be added to limit the molecular weight and hence alleviate the gel effect. Finally, an inhibitor can be added. Oxygen injection is preferred since oxygen permeates through the reactor rapidly. In addition, it is an inexpensive chemical. By varying the amount of oxygen injected, the rate of polymerization can be regulated to maintain the temperature within a narrow range. Batch times will be increased slightly, but more monomer can be processed per batch.

In this work, the emulsion polymerization of poly(methyl methacrylate) is closely examined experimentally and theoretically. Modeling experience developed by previous investigators is drawn upon to derive equations describing particle population, radical conservation, reaction kinetics, and heat and mass transfer. A balance between mathematical rigor and calculational flexibility is sought, so as to include all known phenomena without making the model too complex for practical use. The open-loop process dynamics of a well-stirred batch emulsion polymerization reactor is first simulated. Results of the calculated and experimental closed-loop dynamics are presented to illustrate the efficiency of this control methodology. Molecular weights obtained with and without oxygen injection are compared to determine the effects of this control measure on product specifications.

TYPICAL REACTOR TYPES IN CONTINUOUS EMULSION PROCESSES

Tubular reactors (or plug flow reactors, PFRs) have not been used for emulsion polymerization on a commercial scale mainly because of reactor plugging and emulsion stability problems. Ghosh and Forsyth[2] have investigated polymerizing styrene in a tubular reactor under laminar flow conditions and found that plugging could only be avoided at high emulsifier concentrations. Rollin et al.[3,4] operated the tubular reactor over a wider range of flow rates. Reactor plugging was avoided under turbulent conditions. Maximum reaction rate occurred at the laminar–turbulent flow transition. However, particle agglomeration was found to be significant at high flow rates and resulted in less than complete monomer conversion. Lynch and Kiparissides[5] have successfully modeled polymerization under turbu-

lent conditions, and Vatanatham and Forsyth[6] have investigated some of the scale up factors.

Traditionally, commercial continuous emulsion processes employ either a single continuous stirred tank reactor (CSTR) or a set of CSTRs in series (a train). The principle advantage is that CSTRs, once started up, produce a highly uniform product. The formation of polymer on the wall can be minimized by completely filling the reactor[7] and by eliminating any stagnation zones that may exist. The steady state polymerization rate, conversion, and particle concentration depend upon the mean residence time in the reactor.[7,8] Since new particles are constantly created, a CSTR produces a broader particle size distribution (PSD) than a PFR or a batch reactor.[7,9] However, the PSD can be narrowed by using two or more CSTRs to approach plug flow conditions. Control of PSD is important in many end-use applications (i.e., paints and adhesives) as latex size affects film forming and adhesion properties.[10]

In the actual startup and operation of a continuous emulsion polymerization train, problems inherently associated with CSTRs, i.e., the existence of multiple steady states and limit cycle oscillations, are often encountered. Multiple steady states can lead to reactor runaway and subsequent plugging or loss of equipment if not handled properly. The high rates of reaction and accompanying heat generation in emulsion processes may result in thermal ignition if heat removal is not adequate. The product MWD will thus be broadened. Tight temperature control is essential.

Sustained cycling occurs when particles grow too fast and deplete the available free emulsifier. Particle formation ceases as a result of temporary suspension of micelle nucleation. This slows the rate of polymerization and lowers the conversion. Continuous addition of surfactant replenishes the supply of free emulsifier and particle nucleation resumes. The cycle is repeated when the surfactant is depleted. Oscillations lasting over several average reactor residence times have been observed by Greene et al.[11] and modeled by Kirillov and Ray[12] and Kiparissides et al.[13] Particle growth rates depend upon the concentration of monomer, initiator, and surfactant, and on the propagation rate. Amplitude of the oscillations is influenced by reactor nonisothermal behavior and by the gel effect. The gel effect contributes to the cycling by lowering termination rates and increasing particle growth rates. Higher temperatures increase the rate of propagation, which gives rise to greater oscillations.

In developing an effective control scheme for particle nucleation and reactor control, it is essential to establish the proper time scale. The effectiveness of a feasible control scheme requires control action to be faster than the nucleation time so as to respond adequately to any process perturbations. The total nucleation time t_n to generate a new particle population can be estimated from the batch nucleation time, assuming that termination is instantaneous and that water phase termination is negligible. Then

$$N_p = 0.67\, N_a R_i t_n \tag{1}$$

where R_i is the rate of initiation, N_p is the number of particles nucleated,

and N_a is Avogadro's number. The 0.67 factor accounts for Gardon's findings[14] that 67% of all particles nucleated will still contain the original live radical at the end of the nucleation period. (The remaining 33% of the particles have absorbed two radicals.) If 5×10^{17} particles/L water is taken as a typical concentration, t_n is about 2.3 min at 50°C with [I] = 5×10^{-4} mol $K_2S_2O_8$/L H_2O ($R_i = 5.56 \times 10^{-7}$ mol/L H_2O). Hence, any manipulation of the initiator or surfactant concentration to control particle formation will not be easy in a large reactor. For this reason, very few control schemes exist for commercial CSTRs and batch processes.

LITERATURE REVIEW OF VARIOUS CONTROL STRATEGIES

In this section, current control schemes for both batch and continuous emulsion systems will be reviewed, with special attention paid to conversion and transient control. Little work has been done for batch and semibatch emulsion reactors because of the short nucleation times. Not much can be done once particle nucleation is complete. The main emphasis has been on reproducing identical reaction conditions for each batch. Most control schemes consist of a feed scheduler for starting up, metering reagents, and shutting down. Some sort of temperature and pressure control may also be used. Amrehn[15] has reviewed recent industrial batch control technology. However, trace quantities of inhibitors (not removed in commercial practice) can still cause significant variations from batch to batch.

In continuous emulsion polymerization processes, particles are continually created. This allows the reactor operator to make changes in the feed recipe to obtain the desired product. A major stumbling block in the development of effective control schemes has been the lack of fast, on-line measuring devices and adequate process models. Control strategies are also hampered by long dead times. Temperature, initiator feed, or surfactant addition have been suggested to alleviate reactor cycling and control the monomer conversion, but have been criticized for being slow in response time.

Wismer and Brand[16] varied the reaction temperature over a portion of a CSTR train to control the overall monomer conversion. A feed-forward control scheme using a simple linear process model was used to change the temperatures. The method was implemented using a digital computer for the production of styrene–butadiene rubber and found to give good results. MacGregor and Tidwell[17] have illustrated the importance of careful plant experimentation, and use of empirical (linear) models for simple feedback control in commercial reactors. However, Poehlein and Dougherty[18] have noted that many systems behave nonlinearly with respect to reactor residence time so these techniques are of limited applicability.

Leffew and Deshapande[19] have proposed an analytical predictor method with dead-time compensation to vary the initiator concentration in a train of CSTRs. The model of Kiparissides et al.[13] was used to simulate the nonlinear behavior of vinyl acetate polymerization. At high emulsifier concentrations, the analytical predictor was shown to provide significantly improved conversion control when compared to standard feedback systems during set point and load changes. However, at low emulsifier concentra-

tions, significant oscillations still occurred when particle formation could not be maintained.

Kiparissides et al.[20] developed a suboptimal control strategy using a multivariate stochastic control algorithm. A locally linear model (derived from nonlinear model equations) was integrated to obtain the process response to changes in both initiator and emulsifier feed rates. A quadratic objective function was used to locate the optimum feedback control response for each discrete time interval. An extended Kalman filter was used to compensate for long reactor dead times. Simulation results showed a substantial reduction in the initial startup overshoot, minimized transients during set point and load changes, and reduced sustained oscillations.

Greene et al.[11] experimentally demonstrated that the cycling in CSTRs could be avoided by careful startup. Oscillations occurred when the reactor was started empty, but disappeared when the CSTR was initially filled with deionized water. However, in some cases, significant transients were still observed after a smooth startup, suggesting that steady states may be subject to rapid changes caused by small perturbations in the feed rate or in the feed concentrations.

More recent control strategies have advocated the use of a seed latex in the feed to avoid oscillatory particle nucleation. Berrens[21] used seed produced in another reactor to achieve stable operation of a continuous PVC reactor. Gonzalez[22] used a continuous tubular prereactor to generate the seed for a CSTR. Nomura and Harada[8] proposed optimizing the process by dividing the monomer feed to a CSTR train into two parts. Some of the monomer and all of the water, initiator, and surfactant are initially fed into a small seed polymerizer. A PFR is used as the first stage to maximize particle production. This seed and most of the monomer are then fed into the train. The number of succeeding CSTRs is reduced by obtaining a high concentration of particles. Pollack et al.[23] did a similar study but replaced the PFR with a small CSTR seed generator.

Several new process instruments are also under development for use in continuous flow and batch systems as alarms or monitoring devices. Schork and Ray[24] have developed and tested an on-line tensiometer for measuring the surfactant concentration and devised an on-line densitometer to monitor the monomer conversion. Hamielec et al.[25] have also developed an on-line light scattering device to measure the particle size and concentration. Work is under way to demonstrate the potential of these devices to control undesired reactor transients and runaways.

Chiang and Thompson[26] and more recently Rawlings and Ray[27] have studied the structure of the dynamic behavior of continuous emulsion CSTRs. Both studies support the notion that micelle deprivation is the chief cause of reactor instabilities. Rawlings and Ray also proved the existence of multiple reactor steady states caused by the gel effect and mapped out regions leading to their occurrence. Reactor runaway and periodic cycling can then be avoided by a judicious choice of operating conditions. Good agreement was reached by Rawlings and Ray with the findings of Schork et al.[28]

The number and size of the polymer particles produced have a significant impact on the viscosity, film-forming characteristics, surface wettability,

and other latex properties. Particle number is mainly controlled by the amount of emulsifier used and the initiator loading. The PSD is commonly controlled by the use of an appropriate emulsifier or mixture of emulsifiers for batch systems. Dunn[29] has discussed the choice of surfactant in the preparation of monodisperse latexes. A seed latex can also be used to initiate particle growth to produce a monodisperse latex.

In continuous flow systems, both the particle number and the PSD are controlled by the mean residence time and residence time distribution in a particular reactor. Ueda et al.[30] and Nomura et al.[31] found that, at low residence times, the number of particles generated in a CSTR is limited by the rate of initiation, while, at long times, particle formation is limited by the surfactant concentration. The number of particles is easily controlled by using a seed latex. Degraff and Poehlein[32] have successfully modeled the PSD for styrene emulsion polymerization in a single CSTR. The narrowest PSD is produced under plug flow conditions. As mentioned above, the final PSD in a CSTR train can be narrowed by using more reactors.

Gerrens[33] reported that the PSD could be controlled by how the monomer is fed to a semibatch emulsion reactor. Monomer was added either directly (monomer feed) or as a monomer emulsion (emulsion feed). Emulsion feed was found to produce fewer, but larger particles than either monomer feed or batch polymerization with the same overall charge. The PSD can also be narrower than the other two methods if particle nucleation could be avoided during emulsion feed. If not, emulsion feed produced the broadest PSD. Both the equivalent batch polymerization and monomer feed, however, had faster polymerization rates than emulsion feed since both formed more particles.

Investigators at Diamond Shamrock Corp. found that low PVC plastisol viscosities can be obtained by combining particles of uniform small size with larger size particles. Gardon and Weidner[34] have been able to produce such a bimodal particle distribution by adding emulsifier in two parts to a batch reactor. A seed latex and the initial surfactant are added initially with the monomer to produce large particles. After a delay, a second load of surfactant is added to form micelles which nucleate to form new small particles. A narrow distribution of new particles is achieved by knowing when to stop adding emulsifier (about 10–20% conversion). Gardon and Weidner accurately modeled the heat transferred from the reactor to the jacket cooling water and used an on-line computer to compute the conversion.

The molecular weight of emulsion polymers is easily controlled by the addition of small quantities of chain transfer agent.[35] Mercaptans are commonly used. An alternative method to produce essentially monodisperse polymers is to use a pulsed photoinitiation system.[36] The molecular weight can then be easily controlled by the pulse frequency as growing chains are initiated and terminated on alternating pulses. Extensive work has been done on modeling the molecular weight and molecular weight distribution produced in CSTRs by DeGraff and Poehlein[32] and Nomura et al.[31] and for batch reactors by Min and Ray[37] and Friis and Hamielec.[38]

Since these product specifications (monomer conversion, particle number and size, and polymer MW) are of prime importance, we will first develop a quantitative emulsion polymerization model, and then investigate a rep-

resentative system experimentally to ascertain the influence of oxygen injection control on the overall process behavior.

MATHEMATICAL MODELING OF BATCH EMULSION PROCESSES

Methyl methacrylate is chosen to represent polymerization processes with a strong gel effect. Modified Smith–Ewart kinetics[14] are used to model particle nucleation and particle number while the O'Toole–Stockmayer equation[39] is used to compute the average number of radicals per particle. The gel effect is simulated by the CCS model, while the long chain hypothesis is made and chain transfer to monomer is accounted for. Model development parallels that taken by Gardon.[14,40–44]

Emulsion polymerization of methyl methacrylate can be divided into three regions to facilitate modeling. The reaction mixture consists of monomer droplets, micelles, and polymer particles dispersed in the aqueous phase (see Fig. 1). The initiator, potassium persulfate, is dissolved in the aqueous phase. Micelles are formed by aggregation of the surfactant molecules, sodium lauryl sulfate, once the critical micelle concentration is exceeded. In region I, primary radicals, formed from the thermal decomposition of the water-soluble initiator, are absorbed into the micelles. This process transforms the micelles into polymer particles. Polymerization is assumed to occur only in the particles. At the end of region I, all existing micelles have been converted into polymer particles, and no further particle nucleation can occur.

Region II is characterized by the growth of these particles at the expense of the monomer droplets. Monomer concentration in the particles stays constant due to a balance between surface tension and thermodynamic swelling (from the monomer diffusing from the droplets to the particles). This results in an almost constant rate of polymerization. Particles continue to be active as more radicals enter. Termination of growing chains is traditionally assumed to occur instantaneously when another radical enters a particle already containing one radical, since intraparticle distances are small. By statistical reasoning, half of the particles will be reacting at any one time. This result is one of the key ideas in the Smith–Ewart theory[45] and has been challenged recently. Other theories allowing multiple radicals to coexist in a given particle[46] and for radical desorption[47] have been proposed. Region II ends when the monomer droplets have disappeared completely.

In region III, monomer concentration in the particles begins to decline with conversion, as additional monomer is no longer available to diffuse in. This increases intraparticle viscosity and causes a decrease in the radical termination rate. Onset of the gel effect is now probable. More than one radical can exist inside a given particle due to the hindered termination. This also accelerates the reaction. Polymerization stops when either all the monomer has been consumed or a glass is formed. The final mixture (or latex) will comprise of the continuous aqueous phase and the discrete suspended polymer phase.

Table I summarizes the rather simplified kinetic mechanism. Initiation

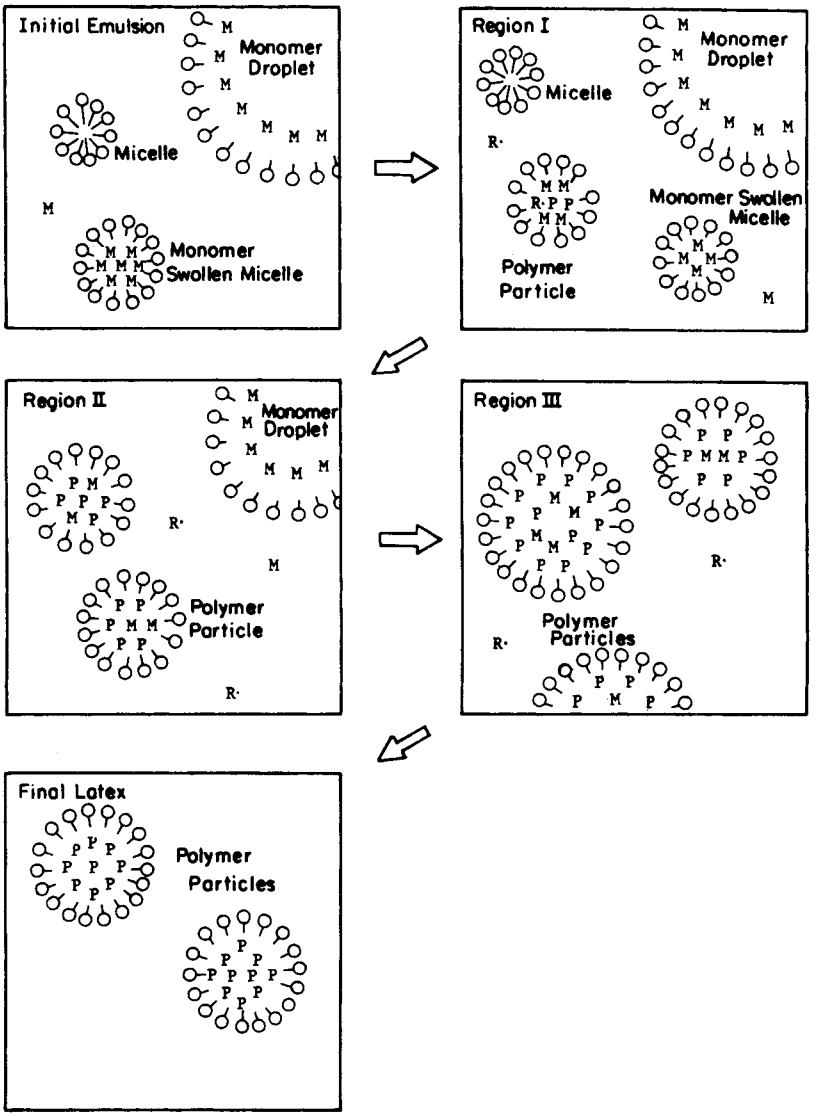

Fig. 1. Schematic representation of an emulsion polymerization process. A typical emulsion (surfactant stabilized droplets) is formed when monomer, surfactant, and water are mixed together. Micelles are formed when the CMC of the surfactant is exceeded. Polymerization begins when a water-soluble initiator is added (region I). Particle nucleation occurs when the monomer swollen micelles are transformed into polymer particles by the entry of a free-radical. Particle nucleation stops when there are no more micelles (region II). Polymer particles then grow at the expense of the monomer droplets. Region III is characterized by the complete depletion of monomer droplets. The reaction then proceeds to completion to form the final latex. (○–) Surfactant molecule; (M) Monomer molecule; (R) Free-radical; (P) Polymer molecule.

is achieved by entry of an aqueous phase primary radical into a micelle or an existing inactive particle. Propagation then proceeds via the addition of monomer molecules to the growing radicals in the particles. Growing polymer chains may transfer their active radical sites to other monomer molecules. Finally, termination by disproportionation occurs when either a primary radical enters a particle with an existing radical or two radicals

TABLE I
Kinetic Mechanism for the Free-Radical Emulsion Polymerization of MMA[a]

Initiation:			
$I_{(aq)}$	$\xrightarrow{k_d}$	$2\,R^{\bullet}_{(aq)}$	
$R^{\bullet}_{(aq)} + M_{(p)}$	$\xrightarrow{k_i}$	$P_1^{\bullet}$	
Propagation:			
$P_j^{\bullet} + M_{(p)}$	$\xrightarrow{k_p}$	$P_{j+1}^{\bullet}$	
Chain transfer:			
$P_j^{\bullet} + M_{(p)}$	$\xrightarrow{k_f}$	$D_j + P_1^{\bullet}$	
Termination:			
$R^{\bullet}_{(aq)} + P_x^{\bullet}$	$\xrightarrow{k_{ii}}$	$D_i + D_x$	[instantaneous termination]
$P_x^{\bullet} + P_y^{\bullet}$	$\xrightarrow{k_t}$	$D_x + D_y$	[disproportionation]

[a] Symbols: $I_{(aq)}$ = water-soluble initiator; $R^{\bullet}_{(aq)}$ = primary radical; $M_{(p)}$ = monomer; $P_j^{\bullet}$ = live radical of chain length j; D_j = dead radical of chain length j; k_d = initiator decomposition rate constant; k_i = radical chain initiation rate constant; k_p = propagation rate constant; k_f = chain transfer to monomer rate constant; k_{ii} = instantaneous termination rate constant; k_t = diffusion controlled termination rate constant.

collide in the same particle. (Termination by combination is ignored.) The latter termination process is only possible during the gel effect region or at high conversions when multiple radicals coexist in the particle.

REGION I

The ensuing analysis is divided into the aforementioned three regions. The major objectives in modeling region I are to develop equations governing the rate of particle nucleation and the final number of polymer particles produced. These equations were first derived by Smith and Ewart[45] and subsequently put on a more fundamental basis by Gardon.[14,40] Derivation of our model equations is summarized below.

To simplify the analysis, the following assumptions are made:

1. Isothermal conditions. This is a reasonable approximation as the conversion is still low (less than 5% conversion) even at the end of region I. Consequently, the small amount of heat released should not significantly raise the reactor temperature.

2. Monomer volume fraction in the polymer particles remains constant, i.e., $\Phi_m = \Phi_m^0$. This is valid since the diffusion of monomer into the particle is fast. Even while the particle grows, the amount of monomer in the particle remains at the thermodynamic equilibrium value.[14]

3. Smith–Ewart kinetics for radical termination. The allowable radical number in any given particle is thus either 0 or 1.

4. Polymerization occurs only in the monomer-swollen polymer particles.

There is a considerable body of data by Fitch and Tsai[48] which indicates that particle formation may actually occur by oligomer growth and agglomeration in the aqueous phase for water-soluble monomers like MMA.

Fortunately, the results with and without micelle nucleation are not too dissimilar, so that the actual mechanism need not be used in the derivation.

All concentrations in the subsequent discussion will be expressed in terms of moles per unit volume of aqueous phase unless otherwise specified. Since both the number of particles and the average number of radicals per particle vary with time, unsteady state balances are required. The rate of particle generation can be found from

$$\frac{dN(t)}{dt} = R_i \frac{\eta A_m}{A_p + A_m} = 2N_a f k_d [\mathrm{I}] \frac{\eta A_m}{A_p + A_m} \tag{2}$$

where A_p is the total particle surface area and [I] is the concentration of initiator. Particle generation is a function of the rate of decomposition of aqueous initiator and the relative rate of radical entry into the micelles. The latter is proportional to the surface area of the micelles, A_m. A surface affinity factor η accounts for the relative ease of radical entry into micelles over particles. The total number of particles per unit volume of water, N, can then be related to the initial initiator and surfactant concentration, through eq. (2). The intermediate steps can be found in Gardon.[14] The final result is

$$N(t) = \eta R_i \left(t - 0.220 \frac{K^2 \eta R_i}{S} - t^{8/3} \right) \tag{3}$$

where

$$S = A_p + A_m = A_s[\mathrm{S}] \tag{4}$$

$$K = \left[(36\pi)^{1/2} \frac{k_p}{N_a} \frac{d_m}{d_p} \frac{\Phi_m^0}{1 - \Phi_m^0} \right]^{1/3} \tag{5}$$

with Φ_m as the volume fraction of monomer in the particles, t as the elapsed time since the start of polymerization, and d_m and d_p as the density of pure monomer and polymer, respectively. The total interfacial area per unit volume of water, S, can be determined from the initial concentration of emulsifier and the area occupied by a mole of surfactant molecules, A_s, in a monolayer film.

Region I ends when the total surface area of the growing particles equals S. At this point, micelles are no longer available for particle generation. The reaction time needed to reach the end of region I, t_I, is given by

$$t_I = \left(\frac{S}{0.587 K^2 \eta R_i} \right)^{3/5} \tag{6}$$

The final number of particles generated, N^0, can be calculated from eq. (3) by setting $t = t_I$:

$$N^0 = 0.860 \left(\frac{\eta R_i}{K^3} \right)^{2/5} S^{3/5} \tag{7}$$

Gardon[14] has experimentally verified the validity of eq. 7 for MMA–SLS (sodium lauryl sulfate)–KPS (potassium persulfate). However, Min and Ray[37] have extensively reviewed the literature and found N^0 to have different dependences for [I] and [S] depending on the initiator and surfactant used. Hence, our model simulations will be only applicable for MMA–SLS–KPS.

Monomer conversion rate is determined by the average number of radicals per particle. The average number can be computed via the following balance equations for radicals in the particles and in the aqueous phase.

$$k_i N^0[\mathrm{R}] - k_i N_1[\mathrm{R}] + \frac{dN}{dt} = 0 = \frac{d\lambda_p}{dt} \tag{8}$$

where $\mathrm{N} = \mathrm{N}_0 + \mathrm{N}_1$, and

$$R_i - k_i N[\mathrm{R}] - \frac{dN}{dt} = 0 = \frac{d\lambda_w}{dt} \tag{9}$$

In the above equations, N_0 and N_1 are the total number of particles with no and one radical, respectively, and λ_p and λ_w are the total radical concentrations inside the particles and in the water phase. The quasi-steady state approximation (QSSA) is used in both equations. Terms on the left-hand side of eq. (8) represent the rate of reactivation of dead particles by entry of a new primary radical, the rate of inactivation of live particles via instantaneous termination with a second incoming primary radical, and the rate of micelle-to-particle transformation. Equation (9) balances the rate of aqueous primary radical generation with the sum of the rates for alternate activation and deactivation of particles and micelles. The average number of radicals per particle can be deduced from eqs. (8) and (9) as

$$\bar{n}(t) = \frac{1 \times N_1 + 0 \times N_0}{N} = \frac{N_1}{N} = \frac{R_i}{2R_i - 2(dN(t)/dt)} \tag{10}$$

Equation (3) is used in conjunction with eq. (10) to obtain the time-dependent average number of radicals per particle.

With the assumption that monomer consumption is largely caused by the propagation step (the long chain hypothesis), the rate of polymerization, R_p, can be calculated by

$$R_p = -\frac{d[\mathrm{M}]}{dt} = k_p[M_p^0]\,\bar{n}(t)\,\frac{N(t)}{N_a} \tag{11}$$

where $[\mathrm{M}_p^0]$ is the monomer concentration per unit volume of particles, and $\bar{n}$ is the average number of radicals per particle. $[\mathrm{M}_p^0]$ is constant in this region by virtue of assumption 2 and can be found by

$$[\mathrm{M}_p^0] = \Phi_m^0 d_m / \mathrm{mw}_m \tag{12}$$

where Φ_m^0 is the volume fraction of monomer in region I, and mw_w corresponds to the molecular weight of methyl methacrylate. The fractional conversion x is defined by

$$x = 1 - \frac{[M] - [M_s]}{[M_0] - [M_s]} \tag{13}$$

where $[M_0]$ is the initial monomer concentration. The slight solubility of the monomer in the aqueous phase, $[M_s]$, has been accounted for in eq. (13). Combination of eqs. 11 and 13 gives the following relationship:

$$\frac{dx}{dt} = \frac{k_p[M_p^0]\bar{n}(t)N(t)}{([M_0] - [M_s])N_a} \tag{14}$$

The cumulative number average molecular weight $\overline{M}_n$ of the polymer produced can be computed by dividing the total weight of converted monomer by the total number of dead chains and growing polymer radicals present in all the particles. The latter quantity is determined from

$$(\Lambda(t) + \bar{n}(t)) = \frac{\int_0^t \{R_i + C_{tm}N_a([M_0] - [M_s])\, dx/dt\}dt}{N(t)} \tag{15}$$

where $C_{tm} = k_f/k_p$ and Λ is the average number of dead chains per particle. In deriving eq. (15), chain transfer to monomer has been considered a chain termination step with simultaneous initiation of a new chain. Accumulation of radicals in the aqueous phase is neglected. The number of dead chains and live radicals is then found from the rate of primary radical generation and the rate of chain transfer. The average molecular weight is then given by

$$\overline{M}_n = \frac{([M_0] - [M_s])\, N_a mw_m x}{(\Lambda(t) + \bar{n}(t))N(t)} \tag{16}$$

The calculation of the cumulative weight average molecular weight $\overline{M}_w$ is deferred to a later section.

REGION II

As all available micelles have been converted to growing polymer particles at the end of region I, the total number of particles per unit volume of water, N, remains constant thereafter. Monomer continues to diffuse into the particles from undepleted monomer droplets to replace the portions of monomer consumed. As a result, Φ_m is again kept constant at Φ_m^0. However, radical termination may no longer be considered instantaneous since particles are now, in general, much larger than before. Hence, a new radical balance equation is needed. Significant amounts of heat may also be generated in this region by the reaction so an energy balance is required to evaluate the reactor temperature.

Since radical termination is mainly determined by the frequency of radical absorption, radical lifetimes are extremely long (about 3 min at 50°C). There is then a distinct possibility of radicals escaping from particles just after a chain transfer reaction. Desorption is possible because monomeric radicals are far more mobile than the larger polymer macroradicals. Desorbed radicals are then either captured by other particles or terminated by reacting with aqueous phase primary radicals. This decreases the rate of polymerization. Another complication arises from the finite termination rate, which may allow more than one radical to coexist in the same particle. This speeds up monomer conversion.

The average number of radicals per particle can be determined from the following unsteady state balance

$$\frac{dN_n}{dt} = \frac{k_i[\mathrm{R}]N_a}{N^0}N_{n-1} + k_e\bar{a}_p\frac{n+1}{\bar{v}}N_{n+1} + k_t\frac{(n+1)(n+2)}{\bar{v}}N_{n+2} - \frac{k_i[\mathrm{R}]N_a}{N^0}N_n - k_e\bar{a}_p\frac{n}{\bar{v}}N_n - k_t\frac{n(n-1)}{\bar{v}}N_n \tag{17}$$

where k_e is the radical desorption rate constant, $\bar{v}$ and $\bar{a}_p$ are the average volume and surface area of a particle, and N_n is the number of particles with n radicals. The first three terms of eq. (17) account for processes transforming particles with $(n + 2)$, $(n + 1)$, and $(n - 1)$ radicals into ones with n radicals while the last three terms correspond to processes changing particles with n radicals into other species. The average number of radicals per particle is then computed from

$$\bar{n} = \frac{\sum_{n=0}^{\infty} nN_n}{\sum_{n=0}^{\infty} N_n} \tag{18}$$

Summation of the infinite series can be truncated after the first few terms as convergence is rapidly reached. Equation (17) has been solved numerically for the first few n radical species,[40] but the results obtained are almost identical to those found when the QSSA is used ($dN_n/dt = 0$).

Smith and Ewart[45] were the first to solve eqs. (17) and (18) analytically for three limiting cases when the QSSA is valid. They found that when radical desorption is significant and termination is slow (case 1), $\bar{n}$ is less than ½. When termination is assumed instantaneous and desorption is negligible (case 2), $\bar{n}$ equals ½. And when both radical desorption and termination are slow (case 3), $\bar{n}$ is greater than ½. Case 1 exists for vinyl acetate and vinyl chloride, while styrene and MMA approximate case 2. Case 3 is applicable to suspension polymerization.

The general solution of Equation (17) without radical desorption was solved by Stockmayer[39] and subsequently reexpressed in a simplier form by O'Toole.[46] The final results are

$$\bar{n} = \frac{a}{4}\frac{I_0(a)}{I_1(a)} \tag{19}$$

where I_0 and I_1 are modified Bessel functions of the first kind of zeroeth and first order, and

$$a = \left\{ \frac{8\ k_i[\mathrm{R}]\bar{v}N_a}{k_t} \right\}^{1/2} \tag{20}$$

$$\bar{v} = \frac{x([\mathrm{M}] - [\mathrm{M}_s])\ \mathrm{mw}_m}{d_p N^0 (1 - \Phi_m^0)} \tag{21}$$

Recently, Ugelstad et al.[47] solved eq. (17) with radical desorption and water phase termination. The concentration of radicals in the water phase, $[\mathrm{R}_w]$, was determined from

$$\frac{d[\mathrm{R}_w]}{dt} = R_i + \sum_{n=0}^{\infty} \frac{k_e \bar{a}_p}{\bar{v}} n N_n - 2k_{tw}[\mathrm{R}_w]^2 - k_i[\mathrm{R}]N^0 = 0 \tag{22}$$

where k_{tw} is the water phase termination rate constant of primary radicals and [R] is the concentration of primary radicals in the particles. Since $\sum_{n=0}^{\infty} nN = \bar{n}N^0$, eq. (22) can be rewritten in dimensionless form,

$$\alpha = \alpha' + m\bar{n} - Y\alpha^2 \tag{23}$$

where

$$\alpha = k_i[\mathrm{R}]N^0\bar{v}/k_t\mathrm{N}^0 \tag{24}$$

$$\alpha' = R_i\bar{v}/k_t N^0 \tag{25}$$

$$m = k_e \bar{a}_p / k_t \tag{26}$$

and

$$Y = 2k_{tw}k_t / k_i^2 N^0 \bar{v} \tag{27}$$

Equations (19) and (22) are then solved simultaneously for $\bar{n}$.

Water phase termination is usually negligible and radical desorption is not significant for MMA, since chain transfer to monomer is relatively slow ($C_{tm} \simeq 10^{-5}$ at 60°C). Thus, eqs. (19)–(21) are sufficient to describe the average number of radicals per particle. The quantity $k_i[\mathrm{R}]$ in eq. 20 can be estimated from an overall radical balance where the rate of radical generation is equated to the rate of radical entry into the particles:

$$R_i = 2N_a f k_d[\mathrm{I}] = k_i N^0[\mathrm{R}] \tag{28}$$

The average number of radicals per particle is slightly larger than ½ and increases with increasing conversion in region II, since multiple radicals can coexist within the same particle as particles grow in size. This has been modeled by making $\bar{v}$ a function of x [see eq. (21)].

Calculation of the fractional conversion is similar to the case of region I, except that now $N(t) = N^0$. This gives

$$\frac{dx}{dt} = \frac{k_p[\mathrm{M}_p^0]\bar{n}N^0}{([\mathrm{M}_0] - [\mathrm{M}_s])N_a} \tag{29}$$

The initial condition for this differential equation is $x = x_\mathrm{I}$ at $t = t_\mathrm{I}$. The strategy used to compute $\overline{M}_n$ is the same as before:

$$\frac{d(\Lambda + \bar{n})}{dt} = k_i[\mathrm{R}] + \frac{C_{tm}N_a([\mathrm{M}_0] - [\mathrm{M}_s])}{N^0}\frac{dx}{dt} \tag{30}$$

and

$$\overline{M}_n = \frac{x([\mathrm{M}_0] - [\mathrm{M}_s])\,N_a\,\mathrm{mw}_m}{N^0(\Lambda + \bar{n})} \tag{31}$$

Both chain transfer and the rate of initiation are expected to play a significant role in determining the polymer molecular weight in region II as both are temperature-sensitive.

The temperature of the reaction mixture is constantly updated by the following energy balance:

$$mCp\frac{dT}{dt} = -\Delta H_p\left(-\frac{d[\mathrm{M}]}{dt}\right)V - UA_c(T - T_s) \tag{32}$$

where m, V, and Cp are the total mass, volume, and average specific heat capacity of the reacting emulsion, U is the overall heat transfer coefficient, A_c is the available surface area, and ΔH_p is the heat of polymerization. Heat generation from the propagation step is assumed to be dominant, and heat effects from initiation, chain transfer, and termination are ignored. (This is consistent with the long chain hypothesis.) Heat removal is accomplished by transfer to cooling water circulating in a constant-temperature, cooling water jacket.

Region II ends when all the monomer droplets disappear. Variables at the end point are denoted by a subscript II in subsequent derivations. The end point is easily determined from a mass balance of monomer since all monomer must reside in the particles at the end of region II. This gives

$$([\mathrm{M}_0] - [\mathrm{M}_s])(1 - x_\mathrm{II}) = N^0\bar{v}_\mathrm{II}\Phi_m^0\,d_m/\mathrm{mw}_m \tag{33}$$

The average volume of the particles is then calculated from the simple relationship

$$\bar{v}_\mathrm{II} = \frac{([\mathrm{M}_0] - [\mathrm{M}_s])\mathrm{mw}_m x_\mathrm{II}}{d_p N^0(1 - \Phi_m)} \tag{34}$$

The last two equations allow x_{II} to be determined as

$$x_{II} = \frac{(1 - \Phi_m^0)}{(1 - \Phi_m^0) + \Phi_m^0 (d_m / d_p)} \tag{35}$$

Now, Equation (29) is integrated numerically until $x = x_{II}$, at which point $t = t_{II}$, and the end of region II is reached.

REGION III

This region differs from region II only in that Φ_m is now a variable. Φ_m will vary with both conversion and temperature, and can be computed from a monomer balance

$$\Phi_m = \Phi_m^0 \frac{d_{mII}}{d_m} \frac{[M_p]}{[M_p^0]} = \Phi_m^0 \frac{d_{mII}}{d_m} \frac{(1 - x)}{(1 - x_{II})} \frac{(1 - x_{II})/d_{mII} + x_{II}/d_p}{(1 - x)/d_m + x/d_p} \tag{36}$$

As before, the subscript II designates prevailing conditions at the end of region II. The density of the polymer, d_p, is assumed independent of temperature since the thermal expansion coefficient of PMMA is small. Equations (19) and (20) can still be used to compute $\bar{n}$, but eq. (21) needs to be slightly modified

$$\bar{v} = \frac{x([M_0] - [M_s])mw_m}{d_p N^0 (1 - \Phi_m)} \tag{37}$$

The conversion can then be obtained from

$$\frac{dx}{dt} = \frac{k_p [M_p] \bar{n} N^0}{([M_0] - [M_s]) N_a} \tag{38}$$

A pronounced gel effect occurs in region III for most vinyl monomers and has been the subject of many investigations.[38,49-52]

Modeling of the reaction is complicated because the acutal onset of the gel effect is not precisely known. In addition, the glass effect occurs in this region and limits the final monomer conversion. While the polymerization inside the particles can be logically viewed as a bulk polymerization process, most modeling approaches have not used constitutive equations for the gel and glass effects derived from bulk data. Instead, new models based on emulsion data only are used so as to avoid scaling the huge differences in MW between bulk and emulsion polymers.

Friis and Hamielec[49] were one of the first to incorporate the gel effect. They proposed that the onset of the gel effect occurred right at the beginning of the polymerization and that the decrease in the termination rate constant is a strong function of conversion.

$$\frac{k_t}{k_t^0} = \left\{ \frac{1}{(1 - x)} \exp(Bx + Cx^2) \right\}^2 \tag{39}$$

where B and C are functions of temperature, initiator loading, and surfactant concentration. Equation (39) was derived by correlating the bulk data of Balke and Hamielec.[53] However, actual forms for B and C were not derived, and this makes the model very empirical. The glass effect was ignored. Sundberg et al.[51] viewed the reaction as a diffusion-controlled process and used a free volume approach similar to that of Ross and Laurence[54] to model both the gel and glass effects.

$$\frac{k_t}{k_t^0} = C \exp\left[A\left(\frac{1}{v_{fcr}^*} - \frac{1}{v_f}\right)\right] \tag{40}$$

$$\frac{k_p}{k_p^0} = D \exp\left[B\left(\frac{1}{v_{fcr}^0} - \frac{1}{v_f}\right)\right] \tag{41}$$

where A,B,C, and D are constants. A critical free volume v_{fcr}^* was used to characterize the transition between segmental and translational diffusion-control, while another critical free volume v_{fcr}^0 marked the onset of the glass effect. Both critical free volumes were used as "fitting" parameters to match emulsion data only. This makes the model somewhat empirical. Harris et al.[52] proposed that chain entaglements caused the gel effect and scaled the constant C in eq. (40) with the weight average molecular weight in an approach similar to that of Martin and Hamielec.[55]

In this study, the CCS model[56] will be used for the gel and glass effects. This model was derived from bulk polymerization data and has been validated over a wide range of conditions. It should therefore be able to describe adequately the reaction inside an emulsified particle. The constitutive expressions have been discussed previously and only the final equations will be shown:

$$\frac{1}{k_t} = \frac{1}{k_t^0} + \frac{\Theta_t \bar{n}/(\bar{v}N_a)}{\exp[2.303\ \Phi_m/(A(T) + B(T)\Phi_m)]} \tag{42}$$

$$\frac{1}{k_p} = \frac{1}{k_p^0} + \frac{\Theta_p \bar{n}/(\bar{v}N_a)}{\exp[2.303\ \Phi_m/(A(T) + B(T)\Phi_m)]} \tag{43}$$

The apparent rate constants embody a reaction limited and a mass transfer limited term. The relative importance is reflected in the characteristic diffusion times, Θ_p and Θ_t. Since mass transfer limitation is considered from the beginning of the polymerization, eqs. (42) and (43) are used throughout all three regions. [For the first two regions, $\Phi_m = \Phi_m^0$. For region III, Φ_m is determined by eq. (36)]

OXYGEN CONTROL

Onset of the gel effect frequently causes a rapid rise in the temperature. Although the high heat capacity of the water phase partially offsets the potential surge induced by the large amount of heat released, molecular weight can nevertheless decrease as a result of increased intitation and chain transfer rates. In addition, the temperature variation can still be

significant at high monomer loadings. This restricts the maximum volume of monomer that may be processed in the reactor.

Poehlein[7] has suggested that strong inhibitors can control the rate of polymerization, and hence vary the rate of heat generation. If a small amount of oxygen is introduced into the system when the temperature begins to climb, the dissolved oxygen in the aqueous phase may combine with primary radicals to form peroxide radicals, rendering them inactive. Alternatively, oxygen dissolved in the particles may terminate growing chains via combination with the polymer radicals to form inactive species. Absorption of the dissolved oxygen into the oil phase is facilitated by the exceedingly small size of the emulsified particles, being on the average 400–800 Å in diameter. Hence, there exists a large surface to volume ratio for oxygen diffusion from the aqueous phase to the particles.

The kinetic steps governing radical deactivation are summarized below:

$$O_{2(aq)} + R_{(aq)}^{\cdot} \xrightarrow{k_{0w}} RO_{2(aq)}^{\cdot} \text{ (inactive)}$$

$$O_{2(aq)} + P_j^{\cdot} \xrightarrow{k_{0p}} P_jO_2^{\cdot} \text{ (inactive)}$$

Both mechanisms reduce the rate of conversion and, consequently, the rate of heat release. The latter mechanism also lowers the molecular weight by terminating growing chains prematurely. There is evidence for vinyl chloride by Garton and George[57,58] that suggests these peroxides are not totally inactive, but react with monomer at very slow rates. Peroxide bonds are then directly incorporated into the polymer backbone. Garton and George found that the thermal stability of the final polymer was decreased. In this study, however, an inactive polymer peroxide radical will be treated as a dead molecule in the calculations.

To determine if mass transfer effects are important, two scaling problems must first be studied. We need to determine (1) how much oxygen will be held up in the gas phase (or gas bubbles) to deliver the required amount of dissolved gas to the water phase, and (2) how rapidly dissolved oxygen diffuses across polymer particles. Answer to the first question will depend on the mass transfer rate of oxygen into water. A uniform dispersion of oxygen can be assumed once the gas has dissolved since agitation is vigorous. Mass transfer limitation across the water–particle interface can be ignored since the interfacial area is very large. Next, termination of growing radicals by oxygen may be a limiting step as gases usually diffuse through polymers very slowly.

Aeration theory is employed to estimate the gas holdup. The design of an adequate sparger for oxygen control is based on work done on microbial fermentors. Moo-Young and Blanch[59] have reviewed most design techniques. Numerical results developed below are relevant for a 0.75-L lab scale reactor with a 1/75 HP agitator (indentical to the reactor used in our experimental studies). The mean bubble diameter d_b, can be estimated from the power input per unit volume (P/V) of the agitator and system physical properties by[60]

$$d_b = 0.7\left[\frac{\delta^{0.6}}{(P/V)^{0.4}\,\rho_L^{0.2}}\right]\left[\frac{\mu_L}{\mu_g}\right]^{0.1} \tag{44}$$

where δ is the surface tension (about 72 dyn/cm^2 for water against oxygen at 25°C) and ρ_L is the density of water. μ_g is the viscosity of the gas (182.7 $\times$ 10^{-6} P) and μ_L is the viscosity of the emulsion (typically about 2.5 cP). Using these values, an average bubble diameter of 0.15 cm is obtained.

The bubble rise velocity u_b is a function of the bubble diameter. For potential flow ($Re_{bubble} >> 1$),

$$u_b = \sqrt{gd_b/2} \tag{45}$$

where g is the gravitional force constant. This gives a bubble rise velocity of about 8.5 cm/s. Since oxygen is only sparingly soluble in water, all the mass transfer resistance is in the liquid film. The liquid film resistance k_L can be found by

$$k_L = [4Du_b/d_b]^{1/2} \tag{46}$$

where D is the diffusion coefficient of oxygen in water (about 2.1 $\times$ 10^{-5} cm^2/s[61].) Using the above values, k_L equals 0.040 cm/s.

With the assumption of Henry's law, the concentration driving force can be estimated from

$$\Delta C^* = (C^*_{liq,2} - C^*_{liq,1})/\ln(C^*_{liq,2}/C^*_{liq,1}) \tag{47}$$

and

$$C^*_{liq} = 0.00001 \times (1 \text{ mol}/18 \text{ cm}^3) \times P(\text{atm}) \tag{48}$$

where the concentration of oxygen in the water is assumed negligible and P is the pressure. If a 0.5 atm pressure-drop is assumed across the reactor and the reactor is not pressurized, the equilibrium concentration of dissolved oxygen at the top and bottom, $C^*_{liq,2}$ and $C^*_{liq,1}$ respectively, are 9 $\times$ 10^{-7} and 5 $\times$ 10^{-7} mol/cm^3. The log mean driving force is then about 7.2 $\times$ 10^{-7} mol/cm^3.

If enough oxygen is added to keep up with the rate of thermal initiation, the oxygen consumption rate, N_{O_2}, is given by

$$N_{O_2} = k_L a_v \Delta C^* = 2fk_d[I] \tag{49}$$

where a_v is the surface area of the oxygen bubbles in a unit volume of solution. Equation (49) assumes that there is a rapid steady-state balance between primary radicals and any dissolved oxygen molecules. For a 50–50 loading of monomer and water, about 1 $\times$ 10^{-6} mol oxygen/L s will be needed at 60°C with [I] $\simeq$ 4 $\times$ 10^{-4} mol/L H_2O. Equation (49) can then be rearranged to solve for a_v. This gives about 0.035 cm^2/cm^3 of solution.

The gas holdup can be estimated from the bubble diameter and the surface area of the bubbles by

$$\Phi = a_v d_b/6 \tag{50}$$

The superficial gas velocity is then determined from an experimental correlation[60]

$$\mu_{sg} = \left\{ \frac{\Phi}{3.21\,(P/V)^{0.47}} \right\}^{1/0.65} \tag{51}$$

For the above conditions, a gas holdup of 8.7×10^{-4} cc of dissolved oxygen per cc water with a superficial velocity of 2.3×10^{-5} ft/s is found. The volumetric flow rate of oxygen can then be computed knowing the cross-sectional area of the reactor, A,

$$\dot{q}_{O_2} = A\,\mu_{sg} \tag{52}$$

For 0.75-L spherical reactor, A is about 241.5 cm^2 so that about 0.17 mL/s will be needed to stop the polymerization. The theoretical minimum oxygen flow rate can be determined by assuming all the oxygen which enters the reactor dissolves completely. Then eq. (52) is used in conjunction with the ideal gas law to compute the flow rate. Only 0.025 mL/s is needed. The difference between the two flow rates escapes with the overhead purge gas. The above results depend on the type of sparger and the propeller design, but, from these calculations, we may safely assume that the actual oxygen flow rate will be about an order of magnitude greater than the theoretical minimum oxygen flow. However, even if most of the injected oxygen escapes with the purge gas, the total delivery rate is still extremely small.

To answer the second question concerning the rate oxygen diffuses across the polymer particle, the diffusivity of oxygen is needed to estimate the rate of oxygen transport. A characteristic diffusion time can be found from

$$t_d = d^2/D \tag{53}$$

where d is the diameter of an average particle. If 1 μm is used as a conservative estimate for d (typical particle sizes range between 500 and 1000 Å in diameter[37]), a characteristic diffusion time of 0.01 s is found sufficient for oxygen to completely permeate the particle. At this rate, the inactivation of live radicals inside a polymer particle may be assumed to occur instantaneously as oxygen and free radical react rapidly with one another. The short diffusion time is made possible by the small particle size.

Oxygen control can be simulated with a slight modification of the previous model equations for an uncontrolled batch reactor. If oxygen permeation into the particles had been slow, oxygen control could have been accounted for by adding a water phase oxygen termination term in eq. 22 using the analytic solutions of Ugestad et al.[47] But the above estimate of the characteristic diffusion time implies that radicals within the particles are also significantly inhibited. Hence, eq. (17) must also be modified.

Since the interfacial area for mass transfer is large, an equilibrium distribution of dissolved oxygen rapidly establishes between the aqueous phase and the organic phase. This gives

$$[O_2]_{aq} = \beta[O_2]_p \tag{54}$$

where β is the distribution coefficient and $[O_2]_{aq}$ and $[O_2]_p$ are the concentrations of dissolved oxygen in the aqueous phase and in the polymer particles, respectively.

The balance of radicals in the particles now takes on the following form:

$$\frac{k_t(n+2)(n+1)N_{n+2}}{\bar{v}N_a} + k_i[R]N_{n-1} + k_{0p}[O_2]_p(n+1)N_{n+1} = \frac{k_t n(n-1)N_n}{\bar{v}N_a} + k_i[R]N_n + k_{0p}[O_2]_p nN_n \tag{55}$$

where k_{0p} is the inhibition rate constant of polymer radicals by O_2. The QSSA has again been used in deriving eq. (55). Terms accounting for the conversion of polymer radicals to dead chains have been added to both sides of the balance. Equation (55) can be easily solved to give $\bar{n}$ by a slight modification of the results previously obtained in eqs. (19), (20), and (37). Solution for the case with oxygen control is

$$\bar{n} = \frac{\sum_{n=0}^{\infty} n\mathrm{N}_n}{\sum_{n=0}^{\infty} N_n} = \frac{a}{4}\frac{I_{-m}(a)}{I_{1-m}(a)} \qquad (\text{for } m \leqslant 1) \tag{56}$$

$$= -\frac{(m-1)}{2} + \frac{a}{4}\frac{I_{m-2}(a)}{I_{m-1}(a)} \qquad (\text{for } m > 1) \tag{57}$$

where

$$a = \left\{\frac{8\, k_i[R]\, \bar{v}N_a}{k_t}\right\}^{1/2} \tag{58}$$

and

$$m = \left\{\frac{k_{0p}\,[O_2]_p\, \bar{v}N_a}{k_t}\right\}^{1/2} \tag{59}$$

Again, knowledge of $k_i[R]$ is required to compute n as indicated in eqs. (56)–(59). This quantity is easily determined through a balance of aqueous phase radicals

$$R_i - k_i[R]N^0 - N_a k_{0w}[R]\,[O_2]_{aq} = 0 \tag{60}$$

assuming the QSSA is valid for eq. (22). Equation (60) can then be rearranged to give

$$k_i[R] = \frac{R_i}{(\zeta[O_2]_{aq} + 1)N^0} = \frac{2N_a f k_d[I]}{(\zeta[O_2]_{aq} + 1)N^0} \tag{61}$$

where

$$\zeta = \frac{N_a k_{0w}}{k_i N^0} \tag{62}$$

and k_{0w} is the inhibition rate constant of primary radicals in the aqueous phase by oxygen. Strictly speaking, ζ is a function of temperature. When oxygen is used to control the reaction, the reactor temperature does not greatly deviate from the set point temperature. Hence, ζ will not change significantly (since both k_{0w} and k_i increase with temperature) and may be assumed constant in the calculations. The rate of reaction, conversion, and $\overline{M}_n$ are calculated as before, except that the new $\bar{n}$ is to be substituted into the appropriate equations.

The remaining tasks are to design an efficient algorithm for feeding oxygen into the reactor and to correlate the amount introduced with the dissolved concentrations in both phases. This latter goal can be achieved by considering an overall oxygen balance. Assuming that all the oxygen introduced is totally dissolved, we have the following equation:

$$\frac{d\{[O_2]_{aq}(1 + N^0\bar{v}/\beta)\}}{dt} = \frac{q}{V}[O_2]_{in} - k_{0w}[R]\,[O_2]_{aq} - k_{0p}[O_2]_p\bar{n}\frac{N^0}{N_a} \quad (63)$$

This equation provides a means to calculate $[O_2]_{aq}$ needed for computing $\bar{n}$ as shown in eqs. (54), (59), and (61). Since the temperature of the system never differs appreciably from the set point, especially when the control strategy works well, β will be taken as a constant. However, it is really a function of temperature.

Since oxygen control is fast, dead time compensation is not needed and simple proportional control can be used. In this scheme, the deviation of the reactor temperature from the set point provides an indicator for regulating the oxygen flow. The total oxygen feed rate is thus given by

$$q[O_2]_{in} \simeq [T - T_{set}] \qquad \text{or} \qquad q \simeq q_0[T - T_{set}] \quad (64)$$

assuming that $T > T_{set}$. If $T \leqslant T_{set}$, no oxygen flow is needed. The actual volume of injected oxygen can be found by using the ideal gas law. Other feed programs, such as on-off and PID control, can also be derived. As discussed above, this calculational method only provides the lower bound of oxygen needed, since the aerator design has been ignored. This deficiency is easily rectified by incorporating a quantitative aeration model.

DETERMINATION OF PRODUCT POLYDISPERSITY

To study the effect of the proposed control method on the polydispersity of the products, we need to compute $\overline{M}_w$ as well as $\overline{M}_n$. The procedure to evaluate $\overline{M}_n$ has been outlined in the previous discussions of polymerization in all three regions. Estimation of $\overline{M}_w$ is more involved. The final equations are nevertheless quite straightforward.

The number of moles of polymer chains formed per unit volume, $\hat{N}$, during an incremental conversion dx is given as

$$d\hat{N} = \frac{d[M]}{\bar{x}_n} = \frac{[M_0]dx}{\bar{x}_n} \quad (65)$$

where $\bar{x}_n$ is the instantaneous number average molecular weight and $[M_s]$ is assumed constant in eq. (13). The total moles of polymer chains produced up to a certain conversion level x is then found by integrating eq. (65) or

$$\hat{N} = \int_0^x d\hat{N} = \int_0^x \frac{[M_0]\, dx}{\bar{x}_n} \tag{66}$$

However, by the definition of $\overline{M}_n$, $\hat{N}$ is also given by

$$\hat{N} = \frac{[M_0]x}{\overline{M}_n} \tag{67}$$

Equating the two expressions yields

$$\overline{M}_n = \frac{x}{\int_0^x dx/\bar{x}_n} \tag{68}$$

Differentiating eq. (68) reverses the result and the instantaneous number average degree of polymerization becomes

$$\bar{x}_n = \frac{dx}{d(x/\overline{M}_n)} = \mathrm{mw}_m \frac{1}{[k_i[R]N(t)/k_p[M_p]\bar{n}N(t)] + C_{tm}} \tag{69}$$

after some work. The term $k_i[R]$ can be evaluated for oxygen control from eq. (61) and without control from eq. (28).

If termination is by disproportionation only, the instantaneous weight average molecular weight can be assumed to be twice the number average, or

$$\bar{x}_w = 2\bar{x}_n \tag{70}$$

Then, for a mixture of differential components, $\overline{M}_w$ may be found by

$$\overline{M}_w = \frac{\int_0^x \bar{x}_w\, dW_p}{\int_0^{W_p} dW_p} = \frac{1}{W_p}\int_0^x \bar{x}_w\, dW_p \tag{71}$$

where W_p is the total weight of polymer formed up to the desired conversion and dW_p is the weight of polymer produced during the incremental conversion dx. However,

$$W_p = W_0 x \quad \text{and} \quad dW_p = W_0\, dx \tag{72}$$

so that

$$\overline{M}_w = \frac{1}{x}\int_0^x 2\bar{x}_n\, \mathrm{dx} \tag{73}$$

where W_0 is the total weight of monomer in the reactor. The product polydispersity is calculated by the defining equation

$$PD = \overline{M}_w/\overline{M}_n \tag{74}$$

This completes the model derivation.

RESULTS AND DISCUSSION

Model predictions for a number of operating conditions will be discussed in this section. These results reveal the influence of various process parameters on conversion, temperature, particle number, and average radical concentration inside the particles. Table II summarizes the polymerization conditions simulated by the model. These encompass practical ranges used in our experiments. Table III lists the model parameters. These have been chosen so as to either conform with literature values (e.g., the kinetic rate constants), or represent best estimates. The base case (i.e., cooling water at 50°C, using an initiator loading at 1 g/L H_2O with 10 g mol MMA/L H_2O, and surfactant concentration of 10 g/L H_2O) will be used for comparison with predictions for other conditions.

Figure 2 shows the conversion history of three runs covering different initiator and surfactant loadings with initial system temperature and cooling water temperature both at 50°C. The arrows mark the transition points between the aforementioned polymerization regions. Curve 1 is the base case. All three curves exhibit a strong gel effect at high conversions. The large heat release associated with the gel effect significantly raises the temperature since the heat transfer coefficient, heat transfer area, and cooling water temperature remain constant. These simulations are based on a 0.75L-L lab scale reactor immersed in a constant temperature bath. Even higher temperature rises are possible in commercial size units since the heat transfer area scales roughly with the 0.6 power of the volume while the rate of heat generation is proportional to the volume. A change in either the initiator or surfactant loading alters the entire conversion history. Decreasing the initiator or emulsifier concentration generates fewer polymer particles than the base case and this reduces the rate of polymerization.

TABLE II
Polymerization Conditions Simulated by the Model

Initiator: potassium persulfate (KPS)
$[I_0]$ = g/L H_2O (3.7 × 10^{-3} g mol/L H_2O)
= 0.5 g/L H_2O (1.85 × 10^{-3} g mol/L H_2O)
Surfactant: sodium lauryl sulfate (SLS)
[S] = 10 g/L H_2O (3.47 × 10^{-2} g mol/L H_2O
= 5 g/L H_2O (1.735 × 10^{-2} g mol/L H_2O
Monomer: methyl methacrylate (MMA)
$[M_0]$ = 375 g/L H_2O (3.75 g mol/L H_2O)
= 600 g/L H_2O (6.0 g mol/L H_2O)
= 1000 g/L H_2O (10.0 g mol/L H_2O)
Temperature of the cooling medium: 50°C and 60°C
Overall heat transfer coefficient: 0.142 Kcal/min-Deg. °C.

TABLE III
Numerical Values of Model Parameters

fk_d	=	$4.362 \times 10^{14} \exp(-33{,}833/RT_k)$	(min^{-1})
k_t^0	=	$5.88 \times 10^9 \exp(-701/RT_k)$	(L/mol min)
k_p^0	=	$2.95 \times 10^7 \exp(-4353/RT_k)$	(L/mol min)
k_{0p}	=	$3.3 \times 10^4\ k_{p0}$	(L/mol min)
k_f/k_p	=	$9.48 \times 10^3 \exp(-13380/RT_k)$	
θ_t	=	$1.1353 \times 10^{-22} \exp(34{,}000/RT_k)/[I_0]$	(min)
θ_p	=	$5.4814 \times 10^{-16} \exp(28{,}000/RT_k)$	(min)
$A(T)$	=	$0.168 - 8.17 \times 10^{-6}\ (T_k - T_{gp})^2$	
$B(T)$	=	0.03	
R	=	1.987 (cal/mol °K)	T_{gp} = 387°K (114°C)
d_p	=	1.2 (g/cm^3)	
d_m	=	$0.973 - 1.164 \times 10^{-3}\ (T_k - 273.15)$	(g/cm^3)
A_s	=	3.0×10^9 (cm^2/mol)	
η	=	0.4	mw_m = 100 (g/mol)
Φ_m^0	=	0.73	V = 750 (mL)
$[M_s]$	=	0.15 (mol/L H_2O)	
UA_c	=	0.142(kcal/min °C)	
$-\Delta H_p$	=	13,800 (cal/mol MMA)	
mC_p	=	$[1000 + ([M_0] - [M_s]) \times 0.33 \times x \times mw_m + ([M_0] - [M_s]) \times 0.49 \times (1 - x) \times mw_m + [M_s] \times mw_m \times 0.49] \times [V/(1000 + [M_0] \times d_m \times mw_m)]$	(cal/°C)
β	=	0.4	
ζ	=	1.0×10^6 (L H_2O/mol)	
T_{set}	=	323 or 333°K (50 or 60°C)	
q_0	=	2.0×10^{-7} (mol/L H_2O min °C)	

Figure 3 examines in detail the particle population dynamics for the three cases at short times. Systems with a lower initiator or surfactant concentration (curves 2 and 3) exhibit a lower final particle concentration than the base case (curve 1). Decreasing the surfactant loading leads to an earlier attainment of the final particle concentration, whereas lowering the initiator loading reduces the rate of particle generation. Even then, only minutes are needed to nucleate all the particles in the batch. The evolution of the average number of radicals per particle is shown in Figure 4. All curves exhibit a sharp increase (approximately 2 orders of magnitude) in the number of radicals per particle towards the end of the reaction. At high conversions (region III), the Smith–Ewart theory is a poor approximation of physical reality. Notice also that only a slight quantitative difference exists among the three cases. Radical concentration inside a representative particle is largely dominated by the apparent termination rate. The slight increase in $\bar{n}$ seen in region II is due to the small decrease in k_t as particles grow. Autoacceleration by the gel effect causes the tremendous increase in $\bar{n}$ seen in region III. The reactor temperature, as discussed above, rises when the gel effect sets in.

The temperature rise, although not overly excessive (being on the order of 10°C), exerts a marked influence on the molecular weight (MW) of the polymer. Figure 2 displays the evolution of the cumulative average MWs and product polydispersity (PD). The initial PD is not 2 (the theoretical value for termination by disproportionation) since the number of radicals

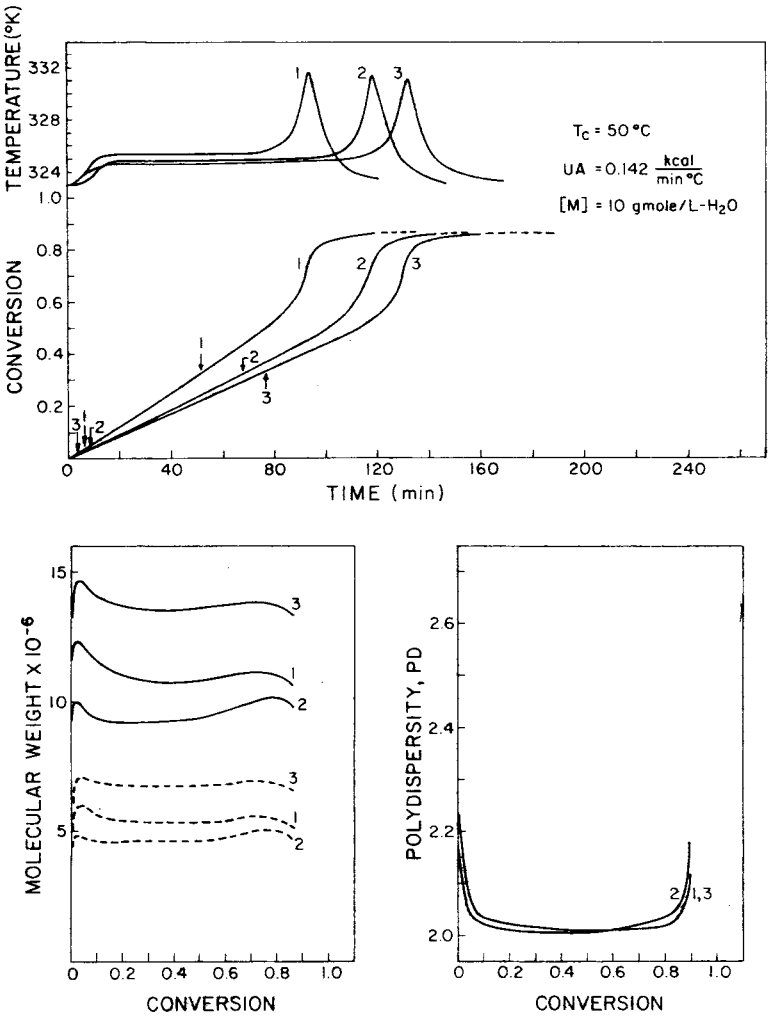

Fig. 2. Calculated temperature, MW, and conversion histories for the nonisothermal batch emulsion polymerization of MMA at different initiator and surfactant loadings. The arrows mark the transitions separating the three regions of emulsion polymerization shown in Figure 1. Model parameters are summarized in Table II. $[I_0]$, $[S_0]$ (g mol/L H_2O): top: (1) 0.0037, 0.0347; (2) 0.00185, 0.0347; (3) 0.0037, 0.01735; bottom right: $[I_0]$, $[S_0]$ (1) 0.0037, 0.0347; (2) 0.0037, 0.01735; (3) 0.00185, 0.0347. Bottom left: (- - -) $\overline{M}_n$; (—) $\overline{M}_w$.

per particle rises first from 0 to 0.833 at the start and then decays to 0.5 at the end of region I. This concentration drift creates an initial MWD which is quite broad and is smoothed over as conversion increases. Both $\overline{M}_n$ and $\overline{M}_w$ decrease after an initial peak as a result of the initial temperature rise. Polymer MWs and PD increase slightly at the end of the reaction due to the gel effect. Decreasing the initiator loading produces longer polymer chains, whereas decreasing surfactant concentration has the opposite effect. Figure 5 shows the importance of chain transfer to monomer on MW predictions. When chain transfer to monomer is absent, the whole MW profile is shifted upwards by a factor of almost 2. The

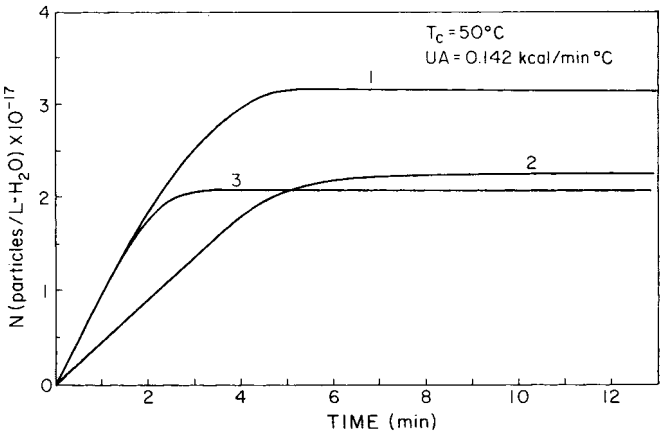

Fig. 3. The rate of particle generation for the emulsion polymerization of MMA at different initiator and surfactant loadings. Note that higher loadings of either surfactant or initiator lead to larger particle densities. $[I_0]$, $[S_0]$: (1) 0.0037, 0.0347; (2) 0.00185, 0.0347; (3) 0.0037, 0.01735.

molecular weight increase due to the gel effect is also more pronounced. PD rises faster in the absence of the chain transfer than with transfer. However, predictions with chain transfer are in better agreement with the data of James and Piirma[62] and those obtained later in this study for PMMA.

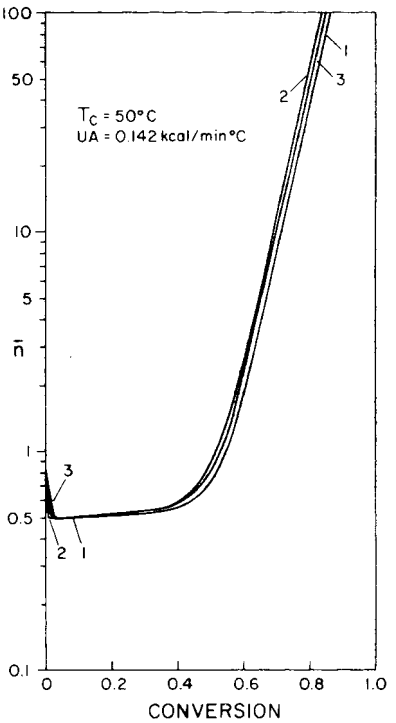

Fig. 4. Calculated average number of radicals per particle as a function of conversion for the three cases shown in Figure 2. $[S_0]$, $[I_0]$ (g mol/L H_2O): (1) 0.0347, 0.0037; (2) 0.01735, 0.0037; (3) 0.0347, 0.00185.

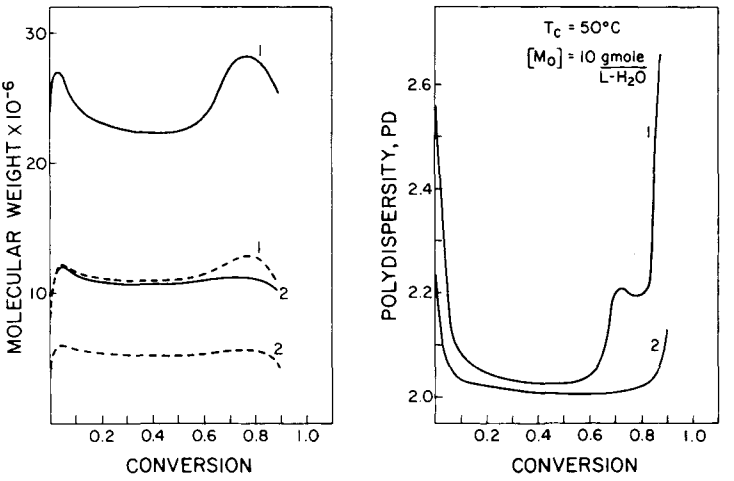

Fig. 5. Influence of chain transfer on the cumulative average molecular weight and polymer polydispersity for the nonisothermal emulsion polymerization of MMA. Note that chain transfer appears to cancel the rise in MW during the gel effect. Left: (- - -) $\overline{M}_n$; (—) $\overline{M}_w$. Right: (1) without chain Transfer (2) with chain transfer.

This is contrary to Min and Ray,[63] who proposed that chain transfer to monomer could be neglected in modeling the emulsion polymerization of methyl methacrylate since radical desorption was negligible. Results of this study indicate that chain transfer to monomer exerts a significant influence on the $\overline{M}_n$ and $\overline{M}_w$ and should be included, especially when very high MWs are encountered.

The effect of varying the monomer loading is shown in Figure 6. Particle nucleation is independent of monomer loading as region I ends at the same time for all three cases. Longer batch times are needed at higher loadings since more monomer must be polymerized. The maximum temperature rise increases with monomer loading as more heat is generated. Polymer molecular weights and product polydispersity both increase at higher loadings.

Changing the initial system temperature and jacket cooling water temperature from 50 to 60°C has a strong influence on the process as shown in Figures 7–10. The rate of conversion is significantly increased at 60°C, as revealed by the conversion histories in Figure 7. Part of the reason for the faster rate is that the number of particles generated increases (see Fig. 8) as more initiator molecules decompose at the higher temperature. Polymer radical mobility is also improved by the higher temperature, facilitating chain termination. As a result, the average number of radicals per particle is less at 60°C than at 50°C. The reaction is accelerated by the large amounts of heat released at the high temperature. The maximum temperature rise shown in Figure 7 is greater at 60°C than at 50°C. The faster reaction rates encountered at elevated temperatures make controlling the reaction much more difficult, since less time is available for control actions. The effects of operating temperature on the product molecular weights are shown in Figure 9. The moderate increase in initial temperature leads to an appreciable reduction in average MWs.

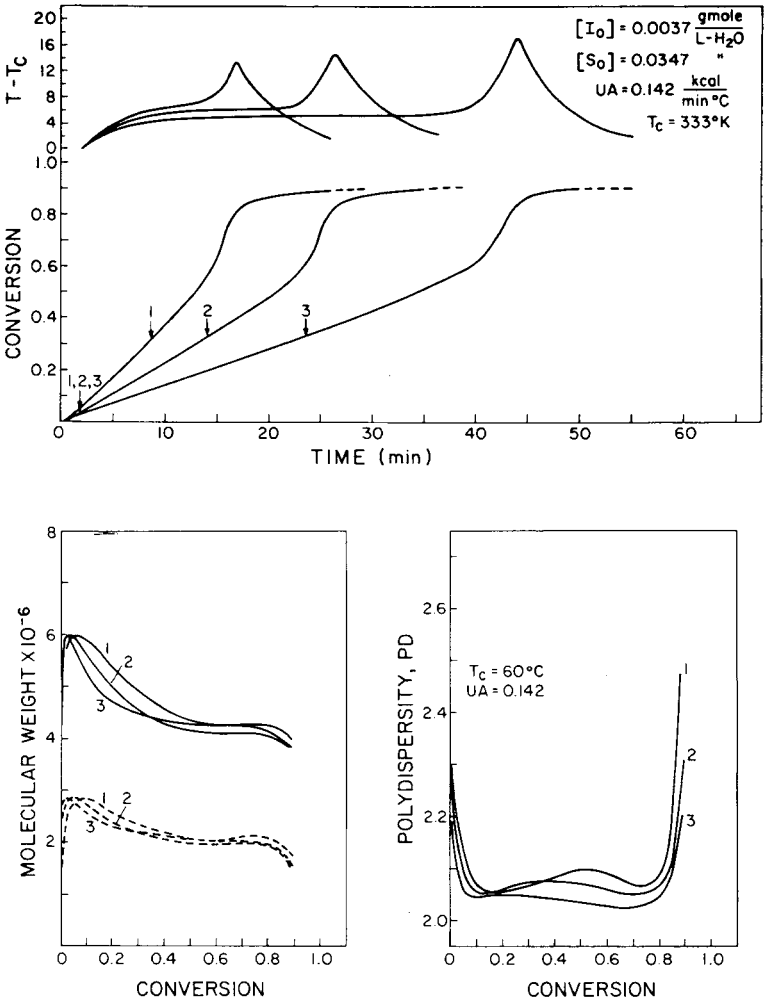

Fig. 6. Influence of monomer loading on the reactor temperature, MW, PD, and monomer conversion for the nonisothermal emulsion polymerization of MMA. Higher loadings require longer batch times. Arrows again mark the transition points between regions of emulsion polymerization. [M] (g mol/L H_2O): top and bottom right: (1) 3.75; (2) 6.00; (3) 10.00. Bottom left: (- - -) $\overline{M}_n$; (—) $\overline{M}_w$.

Since the reaction temperature exerts such a strong influence on the product MW, it is important to control the system temperature within a small tolerance. Proportional control using a small stream of oxygen bubbles can rapidly change the rate of reaction and can eliminate or reduce any temperature rise. Typical results with and without oxygen control are compared in Figures 11–13. Curve 1 is the uncontrolled case. In obtaining these results, the affinity of oxygen to growing radicals was assumed to be much greater than that between monomer and growing radicals. This resulted in an injection rate of about 0.25 mL/min for the reactor under consideration. This number may be an optimistic estimate. However, even in the extreme

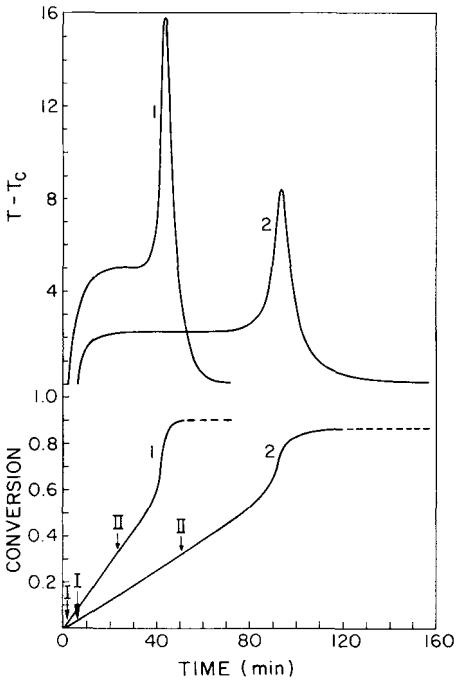

Fig. 7. Influence of coolant temperature on the reactor temperature and conversion during the nonisothermal emulsion polymerization of MMA. The arrows mark the transition betwen different regions of emulsion polymerization. T_c (°C), [I], [S]: (1) 60, 0.0037, 0.0347; (2) 50, 0.0037, 0.0347.

case when the two processes (oxygen termination versus propagation) are equally favored, the required amounts of oxygen is still trivially small.

With controlled oxygen injection, the autoacceleration region can be smoothed out sufficiently as seen in Figure 11. System response to the initial temperature rise is improved by increasing the proportional gain. The ultimate conversion is not affected; only the time needed to obtain it is in-

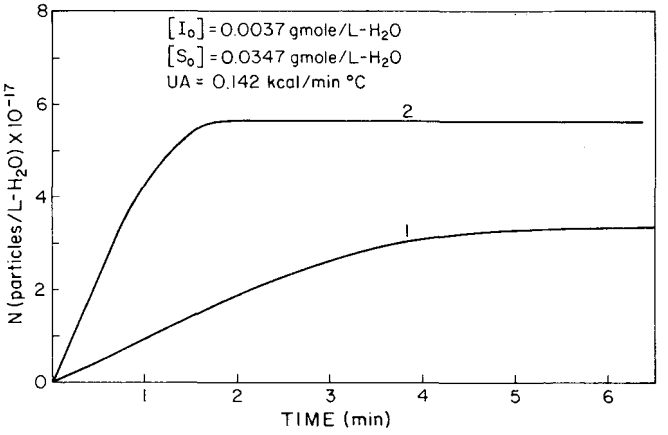

Fig. 8. Total particle population at short times for the emulsion polymerization of MMA for different coolant temperatures (note that higher temperatures lead to faster particle generation rates and larger particle densities). T_c (°C): (1) 50; (2) 60.

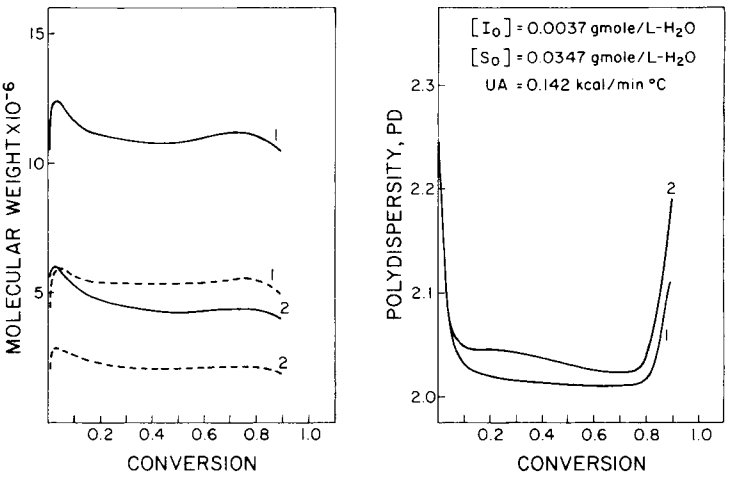

Fig. 9. Evolution of the cumulative average molecular weight and polymer polydispersity as a function of conversion for the nonisothermal emulsion polymerization of MMA at different coolant temperatures. Low MW's are produced at high temperatures. Left: (- - -) M_n; (—) M_w; (1) 50°C; (2) 60°C.

creased. Adding too much oxygen can completely inhibit the polymerization, as demonstrated in curve 4. The average radical concentration in the particles as shown in Figure 13 is greatly reduced by oxygen control. $\bar{n}$ may well drop below that given by the Smith–Ewart theory, 0.5, but increases

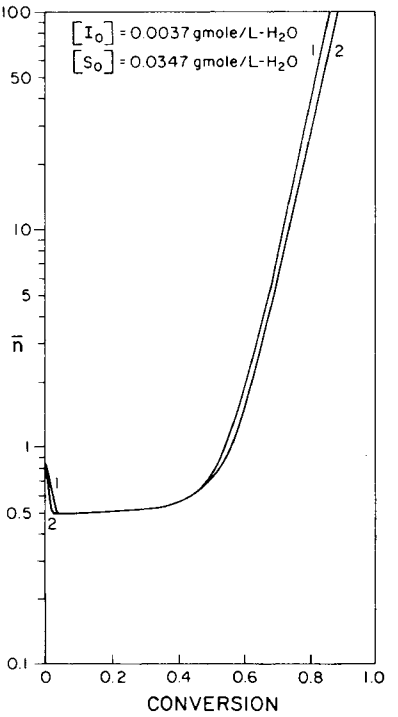

Fig. 10. Calculated average number of radicals per particle as a function of conversion with different coolant temperatures. The average number of radicals greatly increases with conversion due to the gel effect. T_c (°C): (1) 50; (2) 60.

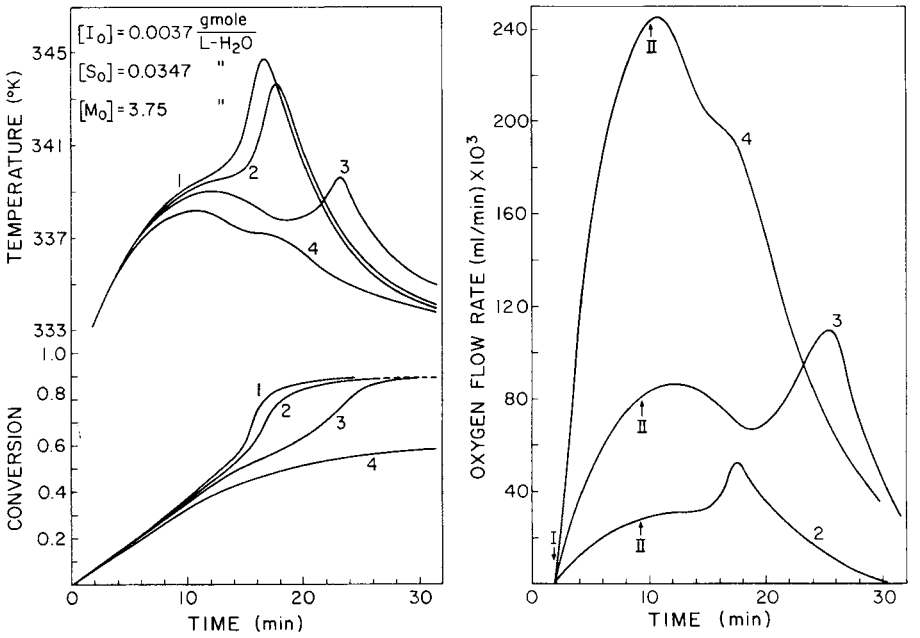

Fig. 11. Comparison of the computed monomer conversion and oxygen injection profiles with and without proportional temperature control for the nonisothermal emulsion polymerization of MMA. Introduction to oxygen reduces the strength of the autoaccelerative gel effect. q_0: left: (1) 0; left and right: (2) 2×10^{-7}; (3) 6×10^{-7}; (4) 2×10^{-6}.

when the gel effect occurs. Although eventually the dissolved oxygen concentration rises sharply when the limiting conversion is approached, this does not present any problem as the monomer is almost depleted and the reaction is limited by the monomer concentration.

Figure 11 shows the temperature history of the reaction mixture with

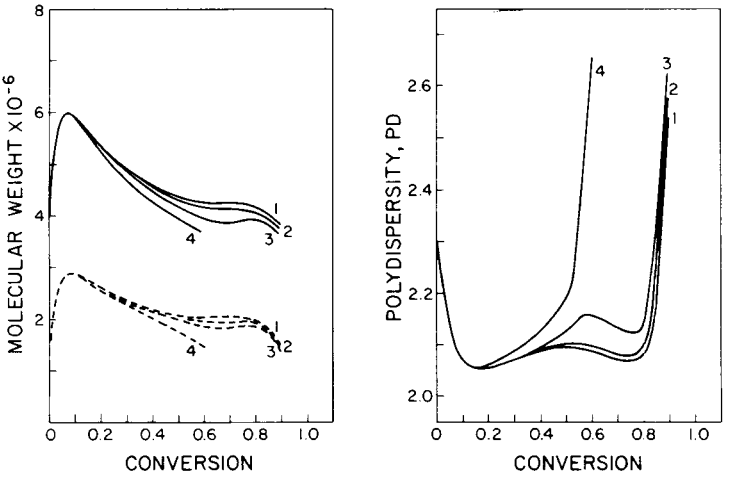

Fig. 12. Comparison of the calculated cumulative average molecular weights and polymer polydispersity with and without proportional temperature control during the nonisothermal emulsion polymerization of MMA. Left: (- - -) $\overline{M}_n$; (—) $\overline{M}_w$ Right: q_0: (1) 0; (2) 2×10^{-7}; (3) 6×10^{-7}; (4) 2×10^{-6}.

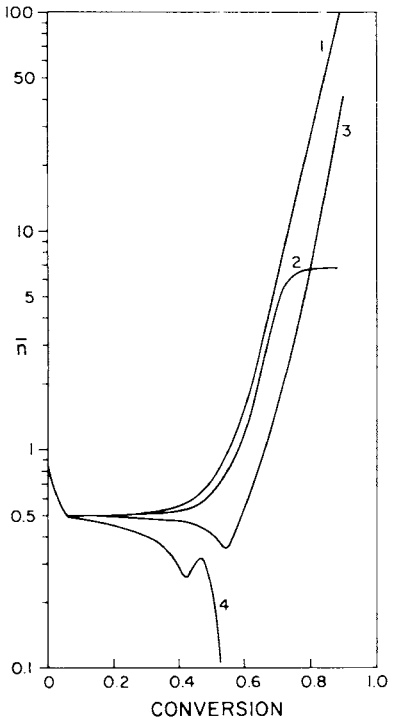

Fig. 13. Influence of proportional temperature control on the average number of radicals per particle. Strong pulses can completely stop all polymerization. q_0: (1) 0; (2) 2×10^{-7}; (3) 6×10^{-7}; (4) 2×10^{-6}.

and without oxygen control. Indeed, the maximum temperature rise around the gel effect region is significantly suppressed. Oxygen injection has a small effect on the temperature variation at low conversions before the gel effect sets in. This is consistent with Figure 13, which shows that the $\bar{n}$ curves are almost identical below 40% conversion. Apparently, for the cases studied, radical concentration inside the particles is dictated by the rate of primary radical entry. Complete isothermal operation is not possible in theory, since there is always a steady state offset with proportional control. However, near-isothermal control may still be possible experimentally, if the inhibition rate constant for primary radicals or the proportional gain has been severely under-estimated in our calculations.

Figure 11 also shows the oxygen injection profiles for the three simulated cases. Oxygen profiles closely mimic the rate of polymerization. Oxygen flows into the reaction immediately after region I ends to limit the temperature rise. Addition rates remain constant in region II and slowly decrease as the polymerization rate falls off in region III. Oxygen delivery rates increase with the gel effect, while onset of the glass effect causes flows to drop. Figure 11 also illustrates that dissolved O_2 can not significantly influence the reactor temperature until the rate of inhibition is comparable to the rate of initiation. In curve 2, initiation is faster than inhibition so a small change in temperature is possible. In curve 4, inhibition is faster than initiation so no reaction can occur. In curve 3, the two rates are comparable, and effective oxygen control is achieved.

The coupled effects of lower temperature and enhanced rate of chain termination on the product MW and PD are seen in Figure 12. Surprisingly, both $\overline{M}_n$ and $\overline{M}_w$ are not appreciably affected by the control measure. The lowered temperature tends to increase the average MWs, whereas deactivation of growing radicals by conversion into peroxide tends to reduce these quantities. The net result suggests that oxygen injection does not cause significant reduction in $\overline{M}_n$ and $\overline{M}_w$. This, however, must be verified by extensive experimentation. The tentative conclusion is that oxygen injection may be a viable and facile control strategy for continuous emulsion polymerization processes without inducing undue molecular weight reduction. If the need arises, oxygen injection can even be used to curtail excessively high product molecular weights.

References

1. C. E. Schildknecht, *Vinyl and Related Polymers,* Wiley-Interscience, New York, 1952.
2. M. Ghosh and T. H. Forsyth, *Am. Chem. Soc.*, **24**, 367 (1976).
3. A. L. Rollin, I. Patterson, R. Huneault, and P. Bataille, *Can. J. Chem. Eng.*, **55**, 565 (1977).
4. A. L. Rollin, I. Patterson, J. Archambault, and P. Bataille, *Am. Chem. Soc. Symp. Ser.*, **104**, 113 (1979).
5. D. Lynch and C. Kiparissides, *J. Appl. Polym. Sci.*, **26**, 1283 (1981).
6. T. Vatanatham and T. H. Forsyth, "Scaleup Factors of Tubular Emulsion Polymerization Reactors," AICHE Annual Meeting, New York, 1977.
7. G. Poehlein, *Am. Chem. Soc. Symp. Ser.*, **104**, 1 (1979).
8. M. Nomura and M. Harada, *Am. Chem. Soc. Symp. Ser.*, **165**, 121 (1981).
9. R. W. Thompson, and J. D. Stevens, *Chem. Eng. Sci.*, **32**, 311 (1977).
10. C. G. Force, in *Emulsion Polymerization,* I. Piirma Ed., Academic, New York, 1982.
11. K. L. Greene, R. A. Gonzalez, and G. W. Poehlein, *Am. Chem. Soc. Symp. Ser.*, **24**, 341 (1976).
12. V. A. Kirillov, and W. H. Ray, *Chem. Eng. Sci.*, **33**, 1499 (1978).
13. C. Kiparissides, J. F. MacGregor, and A. E. Hamielec, *J. Appl. Polym. Sci.*, **23**, 401 (1979).
14. J. L. Gardon, *J. Polym. Sci., Part A,* **6**, 623 (1968).
15. H. Amrehn, *Automatica,* **13**, 533 (1977).
16. D. A. Wismer and W. Brand, Preprints of the Joint Automatic Control Conference, Stanford, CA, 1964, Vol. 5, p. 147.
17. J. F. MacGregor and P. W. Tidwell, *Am. Chem. Soc. Symp. Ser.*, **124**, 251 (1980).
18. G. Poehlein and D. J. Dougherty, *Rubber Chem. Technol.*, **50**, 601 (1977).
19. K. W. Leffew and P. B. Deshpande, *Am. Chem. Soc. Symp. Ser.*, **165**, 533 (1981).
20. C. Kiparissides, J. F. MacGregor, and A. E. Hamielec, *AIChE J.*, **27**, 13 (1981).
21. A. R. Berrens, *J. Appl. Polym. Sci.*, **18**, 2379 (1974).
22. R. A. Gonzalez, M. A. thesis, Department of Chemical Engineering, Lehigh University, Bethehem, PA, 1974.
23. M. J. Pollack, J. F. MacGregor, and A. E. Hamielec, *Am. Chem. Soc. Symp. Ser.*, **197**, 201 (1982).
24. F. J. Schork and W. H. Ray, *Am. Chem. Soc. Symp. Ser.*, **165**, 505 (1981).
25. A. E. Hamielec, C. Kiparissides, and J. F. MacGregor, in *Polymer Colloids II,* R. M. Fitch Ed., Plenum, New York, 1980.
26. A. T. Chiang and R. W. Thompson, *J. Appl. Polym. Sci.*, **24**, 1935 (1979).
27. J. B. Rawlings and W. H. Ray, AIChE Annual Meeting, Los Angeles, 1982, Paper 59g.
28. F. J. Schork, J. B. Rawlings, and W. H. Ray, AIChE Annual Meeting, New Orleans, 1981, Paper 56c.
29. A. S. Dunn, in *Emulsion Polymerization,* I. Piirma, Ed., Academic, New York, 1982.
30. T. Ueda, S. Omi, and H. Kubota, *J. Chem. Eng. Jpn.*, **4**, 50 (1971).
31. M. Nomura, H. Kojima, M. Harada, W. Eguchi, and S. Nagata, *J. Appl. Polym. Sci.*, **15**, 675 (1971).
32. A. W. DeGraff and G. W. Poehlein, *J. Polym. Sci., Part A-2,* **9**, 1955 (1971).

33. H. Gerrens, *J. Polym. Sci., Part C,* **27**, 77 (1969).
34. D. L. Gardon and K. R. Weidner, *Am. Chem. Soc. Symp. Ser.,* **165**, 515 (1981).
35. E. W. Duck, in *Encyclopedia of Polymer Science and Technology,* H. F. Mark, Ed., Wiley-Interscience, New York, 1966, Vol. 5.
36. J. P. Bianchi, F. P. Price, and B. H. Zimm, *J. Polym. Sci.,* **25**, 27 (1957).
37. K. W. Min and W. H. Ray, *J. Macromol. Sci., Macromol. Chem.,* **C11**(2), 177 (1974).
38. N. Friis and A. E. Hamielec, *J. Appl. Polym. Sci.,* **19**, 97 (1975).
39. W. H. Stockmayer, *J. Polym. Sci.,* **24**, 314 (1957).
40. J. L. Gardon, *J. Polym. Sci., Part A,* **6**, 643 (1968).
41. J. L. Gardon, *J. Polym. Sci., Part A,* **6**, 665 (1968).
42. J. L. Gardon, *J. Polym. Sci., Part A,* **6**, 687 (1968).
43. J. L. Gardon, *J. Polym. Sci., Part A,* **6**, 2853 (1968).
44. J. L. Gardon, *J. Polym. Sci., Part A,* **6**, 2859 (1968).
45. W. V. Smith and R. H. Ewart, *J. Chem. Phys.,* **16**, 592 (1948).
46. J. T. O'Toole, *J. Appl. Polym. Sci.,* **9**, 1291 (1965).
47. J. Ugelstad, P. C. Mork, and J. O. Aasen, *J. Polym. Sci., Part A-1,* **5**, 2281 (1967).
48. R. M. Fitch and C. H. Tsai, in *Polymer Colloids,* R. M. Fitch, Ed., Plenum, New York, 1971.
49. N. Friis and A. E. Hamielec, *J. Polym. Sci., Polym. Chem. Ed.,* **12**, 251 (1974).
50. N. Friis and A. E. Hamielec, *Am. Chem. Soc. Symp. Ser.,* **24**, 83 (1976).
51. D. C. Sundberg, J. Y. Hsieh, S. K. Koh, and R. F. Baldus, *Am. Chem. Soc. Symp. Ser.,* **165**, 327 (1981).
52. B. Harris, A. E. Hamielec, and L. Martin, *Am. Chem. Soc. Ser.,* **165**, 315 (1981).
53. S. T. Balke and A. E. Hamielec, *J. Appl. Polym. Sci.,* **17**, 905 (1973).
54. R. T. Ross and R. L. Laurence, *AIChE Symp. Ser.,* **72**, 74 (1977).
55. F. L. Martin and A. E. Hamielec, *Am. Chem. Soc. Symp. Ser.,* **104**, 43 (1979).
56. W. Y. Chiu, G. M. Carratt, and D. S. Soong, *Macromolecules,* **16**, 348 (1983).
57. A. Garton and M. H. George, *J. Polym. Sci., Polym. Chem. Ed.,* **11**, 2153 (1973).
58. A. Garton and M. H. George, *J. Polym. Sci., Polym. Chem. Ed.,* **12**, 2779 (1974).
59. M. Moo-Young and H. W. Blanch, in *Advances in Biochemical Engineering,* Springer-Verlag, New York, 1981, Vol. 19.
60. H. W. Blanch, Course Notes for Chem. Eng. 153, Mass Transfer, Department of Chemical Engineering, University of California, Berkeley, 1983.
61. T. K. Sherwood, R. L. Pigford, and C. R. Wilke, *Mass Transfer,* McGraw-Hill, New York, 1975.
62. H. L. James, Jr., and I. Piirma, *Am. Chem. Soc. Symp. Ser.,* **24**, 197 (1976).
63. K. W. Min and W. H. Ray, *J. Appl. Polym. Sci.,* **22**, 89 (1978).

Received September 20, 1984
Accepted January 16, 1985